Correspondence

Direction-Finding Arrays of Directional Sensors for Randomly Located Sources

The problem of directional sensor placement and orientation is considered when statistical information about the source direction of arrival is available. We focus on two-sensor arrays and form a cost function based on the Cramér–Rao bound that depends on the probability distribution of the coplanar source direction. Proper positioning and orientation of the sensors enable the two-sensor array to have an accuracy comparable to that of a three- or four-sensor uniform circular array.

I. INTRODUCTION

Direction-of-arrival (DOA) estimation is a major topic of antenna-array signal processing, studied extensively over decades [1]. Source parameters (range, polarization, and, most notably, DOA) are extracted from the array manifold with an accuracy that depends on the estimation algorithm but also on the array geometry. The potential of array-geometry adaptation has recently been demonstrated [2–5] to reduce the Cramér–Rao bound (CRB) on the DOA of deterministic/random far/near sources. For instance, (near) optimum nontrivial antenna-array geometries were found that improve DOA estimation accuracy by 36% to 85%, depending on the a priori information available about the source, compared to the more regularly used uniform circular array (UCA) [4].

Similar to previous work [2–5], we continue to consider narrowband sources. However, in this paper, sensors are not omnidirectional, posing the problem of sensor orientations in addition to positions. We continue to refer to the CRB as our performance measure, because it is both algorithm independent and achievable by a number of popular techniques [6, 7]. The CRB is different from one look direction to the other, so we use the expected CRB (ECRB) to build a geometric cost function that also depends on the probability density function (pdf) of the source DOA [2, 4, 8]. Optimization of the analytically intractable CRB-based cost function is achieved by means of a systematic search, preferably to heuristic techniques [2, 8, 9]. In order to reduce the computation burden, a minimal number of two sensors is considered. This is relevant to a number of applications that can accommodate only short-aperture arrays, notably autonomous underwater vehicles used in, for example, adaptive sampling networks [10, 11].

We focus on DOA estimation accuracy and, for instance, do not take array ambiguities into consideration.

Manuscript received September 16, 2015; revised December 31, 2015; released for publication December 31, 2015.

DOI. No. 10.1109/TAES.2016.150655.

Refereeing of this contribution was handled by K. Wong.

First, array ambiguities are less frequent when arrays of directional sensors are used [12]. Second, they can be avoided by an appropriate choice of the spacing between adjacent sensors [12], which is allowed by the proposed algorithm. We also assume a source in the array plane. This is meaningful to a number of terrestrial applications [12–14] and amounts to prioritizing the azimuth angle. With the azimuth as our unique parameter of interest, we develop a scalar-valued performance measure and conduct an optimization in this perspective.

When the response of the directional sensors is not specified, the CRB has a noninterpretable expression [12]. It is only once we assume a specific type of sensor, as in [12, 14], that performance analysis (and optimization) can be conducted. In our tests, we consider cardioid-type sensors for both the proposed geometry-optimized two-sensor array and the reference larger-sized UCAs. In the pessimistic case when there is no information about the source DOA, a scenario studied in [12], we find that sensors should be pointing in different directions, so that the CRB is finite at every possible look direction and the subsequent ECRB is finite as well. If the source DOA is known with (moderate) uncertainty, the optimized two-sensor array has a better accuracy than the three-sensor UCA. The fact that we can achieve with two sensors an accuracy normally achievable by (a UCA of) three sensors implies significant reduction of the size, weight, power, and cost of the system [12], since every single sensor requires a separate receiver channel.

The paper is organized as follows. In Section II, we introduce the observation model and develop expressions of the CRB. In Section III, the CRB of the array of two directional sensors is studied in detail and a subsequent geometry optimization procedure is defined. In Section IV, tests are conducted using cardioid-type sensors to compare the optimized array to larger size UCAs. Finally, a conclusion is given in Section V.

II. SIGNAL MODEL AND GENERAL RESULTS

A narrowband source is emitting a signal $s(t)$ of wavelength λ in the direction of an array of M coplanar sensors. In the $[O, x, y)$ plane, sensor m is placed at point P_m with a distance $OP_m = \rho_m\lambda$ from the origin O and an angle ϕ_m between the $[O, x)$ axis and $[O, P_m)$. The far-field source is seen at the antenna array under the DOA angle θ, restricted to be in $[-\pi, \pi]$, with respect to the $[O, x)$ axis. All angles are measured counterclockwise. The array output at time index t,

$$\mathbf{x}(t) = \mathbf{a}(\theta)\, s(t) + \mathbf{n}(t), \quad t = t_1, \ldots, t_N,$$

is a scaled and noise-corrupted replica of the DOA-dependent array response vector (ARV) $\mathbf{a}(\theta)$. The ARV is an extension of the array steering vector that incorporates gains of the sensors [15]. Its mth component is given by

$$[\mathbf{a}(\theta)]_m = g_m(\theta) \exp[j2\pi\rho_m \cos(\theta - \phi_m)], \quad (1)$$

where we have assumed that sensor m, not necessarily omnidirectional, has a directional response described by the function $g_m(\theta)$.[1]

Snapshots $(\mathbf{x}(t))_{t=t_1,\ldots,t_N}$ are used to estimate the parameter θ using a variety of techniques. The CRB [16] often serves as a benchmark to compare estimation performance of the different estimation algorithms. It represents the lowest mean square error achievable by any unbiased estimator. The CRB is also of practical importance [13] because (in the single-source case considered here) it is achieved (asymptotically, as the number of snapshots increases) by both the high-resolution MUSIC algorithm [6] and the low-resolution beam-forming techniques [7]. The following statistical properties are often assumed about $s(t)$ and $\mathbf{n}(t)$:

1) They are independent.
2) The values $(\mathbf{n}(t))_{t=t_1,\ldots,t_N}$ are independent, zero-mean circular Gaussian distributed with covariance $\mathrm{E}[\mathbf{n}(t)\mathbf{n}^{\mathrm{H}}(t)] = \sigma_n^2\mathbf{I}$, $\mathbf{I}$ being the $M \times M$ identity matrix.
3) The values $(s(t))_{t=t_1,\ldots,t_N}$ are assumed to be either deterministic unknown parameters (the so-called conditional or deterministic model) or independent zero-mean circular Gaussian distributed with variance σ_s^2 (the so-called unconditional or stochastic model). These conditions, while of common use in performance analysis (see, e.g., [16]), do not account for some practical aspects (spatially or temporally correlated noise, mutual coupling, etc.) whose impact is to be evaluated empirically, rather than analytically, which is beyond the scope of this study. The CRBs associated with both models have been proved in [5] to be proportional (one to the other).[2] For instance, the CRB associated with the first model is given by

$$\mathrm{CRB}(\theta) = \frac{\sigma_n^2}{2N\sigma_s^2} F^{-1}(\theta), \quad (2)$$

where, given $\mathbf{a}'(\theta) \triangleq d\mathbf{a}(\theta)/d\theta$, the scalar-valued

$$F(\theta) = \left\|\mathbf{a}'(\theta)\right\|^2 - \frac{\left|\mathbf{a}^{\mathrm{H}}(\theta)\,\mathbf{a}'(\theta)\right|^2}{\|\mathbf{a}(\theta)\|^2} \quad (3)$$

is a convenient design criterion because it is independent from the noise/signal power and the number of snapshots. Consequently, we will be referring to these expressions throughout the paper.

III. THEORETICAL DEVELOPMENT

A. Optimization Criterion

The array is made of two directional sensors [17]. One is placed at the origin, but the position of the other one, characterized by distance $\rho \triangleq \rho_2$ and angle $\phi \triangleq \phi_2$, is to be determined, along with the orientation of each sensor.

[1] Similarly to [12], the sensor response $g_m(\theta)$ is a voltage or current gain, different from the sensor power response $g_m^2(\theta)$.
[2] They are equal if $\|\mathbf{a}(\theta)\|^2\sigma_s^2 \gg \sigma_n^2$.

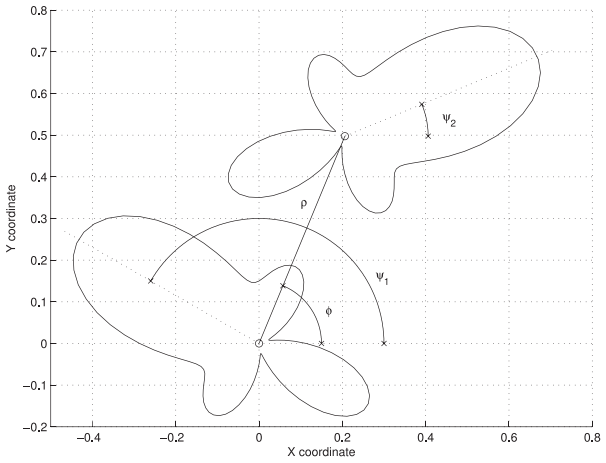

Fig. 1. Positions and orientations of two directional sensors for arbitrarily shaped sensor response $g(\theta)$. Lines show individual responses for each sensor.

Given the expression

$$\mathbf{a}(\theta) = \left[g_1(\theta), g_2(\theta)\exp\left[j2\pi\rho\cos(\theta-\phi)\right]\right]^{\mathrm{T}}, \quad (4)$$

of the ARV, we prove in Appendix A that

$$F(\theta) = g_1^2(\theta)\frac{\left[h'(\theta)\right]^2 + 4\pi^2\rho^2 h^2(\theta)\sin^2(\theta-\phi)}{1+h^2(\theta)}, \quad (5)$$

where $h(\theta) \triangleq g_2(\theta)/g_1(\theta)$, assuming none of the sensors has a strictly zero gain at any direction. Here, $h'(\theta)$ can be interpreted as a measure of the mismatch between the two sensors' directivity patterns. Based on (5), we can make the following two remarks:

1) If the two sensors are identical and pointing in the same direction, $g(\theta) = g_1(\theta) = g_2(\theta)$, then $F(\theta) = 2\pi^2 g^2(\theta)\rho^2\sin^2(\theta-\phi)$ is zero when the source is at the array end-fire direction (i.e., $\theta = \phi$), regardless of how the sensors are directed.

2) In contrast, if the two sensors have different directivity patterns, $F(\theta)$ can be made arbitrarily high provided that $h'(\theta)$ is large enough, including for $\theta = \phi$. In other words, sources that are in the array end-fire direction can be precisely identified only if we use different or differently oriented sensors.

In practice, we are likely to use identical sensors pointing at different directions—i.e.,

$$g_m(\theta) \triangleq g(\theta-\psi_m), \quad m = 1, 2.$$

As illustrated in Fig. 1, the array configuration is now parameterized by geometrical parameters ρ, ϕ, ψ_1, and ψ_2, in function of which $F(\theta)$ is expressed as

$$F(\theta) = \frac{\left[\frac{g'(\theta-\psi_1)}{g(\theta-\psi_1)} - \frac{g'(\theta-\psi_2)}{g(\theta-\psi_2)}\right]^2 + 4\pi^2\rho^2\sin^2(\theta-\phi)}{\frac{1}{g^2(\theta-\psi_1)} + \frac{1}{g^2(\theta-\psi_2)}}. \quad (6)$$

This function is to be interpreted as the ability of the antenna array to accurately localize a source with the specific DOA θ. Since the source DOA cannot be (exactly) known in advance, the overall array performance is more suitably measured in terms of the ECRB [2, 4, 8], defined as ECRB $\triangleq$ E[CRB(θ)]. By adopting the ECRB as a performance criterion, we implicitly allow the CRB to be high at directions where the source is less likely to show up. The a priori information about the source DOA is available in the form of a pdf $f(\theta)$, leading to

$$\mathrm{ECRB} = \frac{\sigma_n^2}{2N\sigma_s^2}\int_{-\pi}^{\pi}\frac{f(\theta)}{F(\theta)}d\theta.$$

Minimizing the ECRB for fixed powers σ_n^2 and σ_s^2 and number N of snapshots is tantamount to minimizing

$$\frac{2N\sigma_s^2}{\sigma_n^2}\mathrm{ECRB} = \int_{-\pi}^{\pi}\frac{f(\theta)}{F(\theta)}d\theta. \quad (7)$$

B. Optimization Procedure

Intersensor spacing ρ is assumed to be fixed based on considerations other than estimation accuracy (e.g., coupling and ambiguity considerations), independently from ψ_1, ψ_2, and ϕ, which remain to be determined by minimization of the ECRB criterion. This is to be achieved by means of a 3-D systematic search. It will be possible to reduce the search area thanks to some properties of the cost function. In fact, (6) is unchanged if ϕ is replaced by $\phi + \pi$ or (ψ_1, ψ_2) is replaced by (ψ_2, ψ_1). Consequently, the systematic search can be restricted to ϕ in $[-\pi/2, \pi/2]$, ψ_1 in $[-\pi, \pi]$, ψ_2 in $[-\pi, \pi]$, and $\psi_1 \le \psi_2$. Notice that, for the sake of numerical stability, configurations where $\psi_1 = \psi_2$ are not tested, because then the function $1/F(\theta)$ is divergent (at $\theta = \phi$), as is the ECRB.

Further simplification is possible if both the sensor response and the DOA pdf are even—i.e., respectively, $g(-\theta) = g(\theta)$ and $f(-\theta) = f(\theta)$. Under these assumptions, we have

$$\frac{2N\sigma_s^2}{\sigma_n^2}\mathrm{ECRB} = \int_0^{\pi}\left\{\frac{\frac{1}{g^2(\theta-\psi_1)} + \frac{1}{g^2(\theta-\psi_2)}}{\left[\frac{g'(\theta-\psi_1)}{g(\theta-\psi_1)} - \frac{g'(\theta-\psi_2)}{g(\theta-\psi_2)}\right]^2 + 4\pi^2\rho^2\sin^2(\theta-\phi)} + \frac{\frac{1}{g^2(\theta+\psi_1)} + \frac{1}{g^2(\theta+\psi_2)}}{\left[\frac{g'(\theta+\psi_1)}{g(\theta+\psi_1)} - \frac{g'(\theta+\psi_2)}{g(\theta+\psi_2)}\right]^2 + 4\pi^2\rho^2\sin^2(\theta+\phi)}\right\} f(\theta)d\theta,$$

so that the ECRB is unchanged if ψ_1, ψ_2, and ϕ are replaced, respectively, by $-\psi_1$, $-\psi_2$, and $-\phi$. It follows that, for such a case, we can further restrict ϕ to be in $[0, \pi/2]$.

IV. OPTIMIZATION RESULTS

The proposed array (which we refer to as CAM[3]) is compared to larger size UCA arrays. In all examples, an intersensor spacing of half a wavelength is assumed, in order to avoid (first-order) array ambiguities [18, 19]. The optimization problem depends on the type of sensors (assumed in Section IV-B to be cardioid) and the distribution of the source azimuth angle (assumed in Sections IV-C and IV-D to be uniform and normal, respectively, to describe worst-case and realistic scenarios). The resolution of the systematic search grid is set to 2 deg. We start by presenting some results about the reference UCA.

A. The Reference UCA

We test our geometry-optimized two-sensor array simultaneously with the commonly used UCA, made of $M = 3, 4, 5, \ldots$ directional sensors. For the UCA, sensors are placed uniformly along the circle—i.e., at angles $\phi_m = 2\pi\ (m-1)/M,\ m = 1, \ldots, M$. The circle radius is $R\lambda$ where $R = \rho/[2\sin(\pi/M)]$ ensures an intersensor spacing equal to ρ. As pointed out in [12], one can avoid array ambiguities in a UCA by appropriately choosing the intersensor spacing ρ. The directional sensors are pointed in the same direction as the sensors—i.e., $g_m(\theta) = g(\theta - \phi_m)$—a fixed-geometry design previously proposed in [12, 14, 20]. The UCA geometry is special in that it verifies, for all k not a multiple of M,

$$\sum_{m=1}^{M} \exp(k\phi_m) = 0, \tag{8}$$

which will be useful to obtain the compact CRB expressions (10) and (13)–(16).

Isotropy is a desired feature of antenna arrays that is fulfilled by UCAs when they are composed of omnidirectional sensors [3]. Interestingly enough, we prove that UCA isotropy may be preserved even when the constituent sensors are not isotropic. We focus our attention on sensors with an arbitrary but symmetrical (even) pattern $g(\theta)$, which are widely encountered in practice. For such sensors, we can write

$$g(\theta) = g_0\left[1 + \sum_{k=1}^{K} \beta_k \cos(k\theta)\right], \tag{9}$$

where $(\beta_k)_{k=1,\ldots,K}$ satisfy $1 + \sum_{k=1}^{K} \beta_k \cos(k\theta) \geq 0$ for all θ, and $\beta_1 \geq 0, \ldots, \beta_{K-1} \geq 0, \beta_K > 0$, hence ensuring a maximum gain in the (0-deg) look direction. Coefficients $\beta_k, k = 1, \ldots, K$, can be easily computed by means of a (truncated) Fourier cosine expansion of $g(\theta)$, whether $g(\theta)$ is available in analytical or numerical form.

We prove in Appendix B that if the directional sensor has a symmetric response $g(\theta)$ as in (9), then the UCA made of M such sensors is isotropic if $M > 2(K+1)$, and it then verifies

$$F(\theta) = \frac{Mg_0^2}{2}\left[\sum_{k=1}^{K} k^2\beta_k^2 + \pi^2R^2\left(4 + \beta_1^2 - 4\beta_2\delta_{K>1} + 2\left(\sum_{k=2}^{K}\beta_k^2\right)\delta_{K>1} - 2\left(\sum_{k=1}^{K-2}\beta_k\beta_{k+2}\right)\delta_{K>2}\right)\right], \tag{10}$$

where $\delta_A = 1$ if condition A is satisfied and 0 otherwise.

Before we interpret this result, we first mention that there is no direct relationship between directivities of the sensors—defined as $D \triangleq [\max_\theta g^2(\theta)]/[(1/2\pi)\int_{-\pi}^{\pi} g^2(\theta)d\theta]$—and isotropy of the UCA, except for specific families of patterns. For example, consider sensors from [12] with response $g(\theta) = g_0[1 + \cos(\theta)]^K$, whose directivity, which is proved in Section IV-C to be equal to

$$D = 2^{4K}\Bigg/\sum_{\ell=0}^{K}\frac{(2K)!2^{2(K-\ell)}}{(\ell!)^2(2(K-\ell))!}, \tag{11}$$

increases with K ($D = 1$, 2.66, 3.66, 4.43, and 5.68, respectively, for $K = 0$, 1, 2, 3, and 4). By application of (10), a minimum of $1 + 2(K+1)$ such sensors is needed to make the UCA an isotropic one. The result in (10) contrasts with the UCA of omnidirectional sensors that is isotropic if $M > 2$ [21]. It proves that a UCA with directional sensors (regardless of how much directional they are) can still be isotropic if the number of sensors is sufficiently large.

Of special interest are cardioid sensors, of frequent use in acoustic systems [22]. They are characterized by a directional response of the form [23]

$$g(\theta) = g_0[1 + \beta\cos(\theta)], \tag{12}$$

parameterized by constants g_0 and β. Application of (10) implies that the UCA is isotropic if populated with five or more such sensors. Then it verifies

$$F(\theta) = \frac{Mg_0^2}{2}\left[\beta^2 + \pi^2R^2\left(4 + \beta^2\right)\right],$$

consistent with [21] for omnidirectional sensors ($\beta = 0$). For completeness, in order to also address a nonisotropic UCA of cardioid sensors, we prove in Appendix D the following expressions for an arbitrarily sized UCA of cardioid sensors:

$$\frac{2F(\theta)}{g_0^2} = 4\sin^2(\theta)\left\{\beta^2 + \cos^2(\theta)\left[\pi^2\rho^2\left(4 + \beta^2\right) - \beta^2\frac{\beta^2 + 4\pi^2\rho^2}{1 + \beta^2\cos^2(\theta)}\right]\right\}, \quad M = 2 \tag{13}$$

$$= \pi^2\rho^2\left[4 + \beta^2 - 4\beta\cos(3\theta) - \frac{\beta^4\sin^2(3\theta)}{2 + \beta^2}\right] + 3\beta^2, \quad M = 3 \tag{14}$$

$$= 4\beta^2 + 4\pi^2\rho^2\left[2 + \beta^2\sin^2(2\theta)\right], \quad M = 4 \tag{15}$$

[3]So named in reference to the chameleon, whose eyes can rotate and move independently from each other.

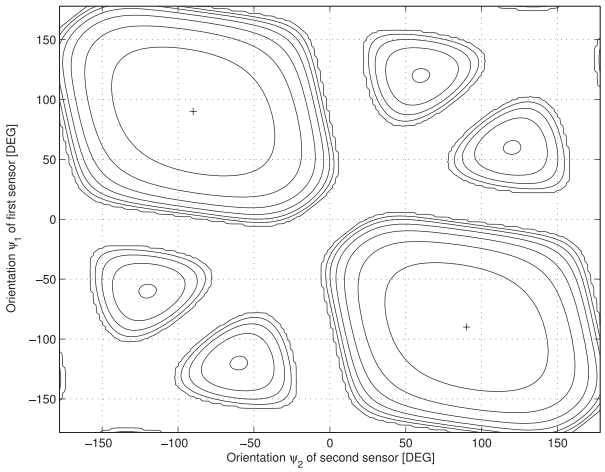

Fig. 2. Cost function C for $\beta = 0.8$. Global minima are shown with $+$ symbols.

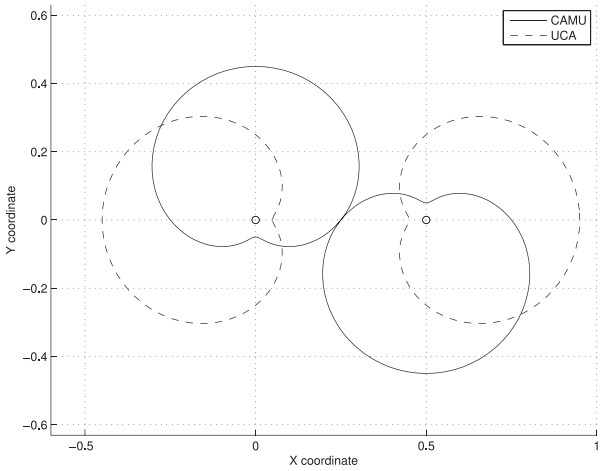

Fig. 3. Sensor orientations of CAMU and UCA2 arrays in (x, y) plane. Sensor positions, shown with circles, are same for both arrays. Lines show individual responses for each sensor when $\beta = 0.8$.

$$= M\left[\beta^2 + \pi^2\rho^2\frac{1+\frac{\beta^2}{4}}{\sin^2\left(\frac{\pi}{M}\right)}\right], \quad M > 4. \tag{16}$$

B. Sensors

In our tests, we consider cardioid-type sensors as defined in (12), parameterized by constants g_0 and, more importantly, β, which controls the sensor directivity D. Directivity D has been found to be equal to $(1+\beta)^2/(1+\beta^2/2)$, which increases from 0 to 2.66 when β increases from 0 to 1. Substituting (12) into (6) leads to the following update of $F(\theta)$:

$$\frac{F(\theta)}{g_0^2} = \frac{\beta^2\left[\frac{\sin(\theta-\psi_1)}{1+\beta\cos(\theta-\psi_1)} - \frac{\sin(\theta-\psi_2)}{1+\beta\cos(\theta-\psi_2)}\right]^2 + 4\pi^2\rho^2\sin^2(\theta-\phi)}{\frac{1}{[1+\beta\cos(\theta-\psi_1)]^2} + \frac{1}{[1+\beta\cos(\theta-\psi_2)]^2}}, \tag{17}$$

where the right-hand side, advantageously, depends on β only, as long as the sensor is concerned. Hence, we adapt the initial criterion (7) to minimize, instead, $(2g_0^2N\sigma_s^2/\sigma_n^2)$ECRB given by the β-dependent

$$C \triangleq \int_{-\pi}^{\pi} \frac{\left(\frac{1}{[1+\beta\cos(\theta-\psi_1)]^2} + \frac{1}{[1+\beta\cos(\theta-\psi_2)]^2}\right) f(\theta)}{\beta^2\left[\frac{\sin(\theta-\psi_1)}{1+\beta\cos(\theta-\psi_1)} - \frac{\sin(\theta-\psi_2)}{1+\beta\cos(\theta-\psi_2)}\right]^2 + 4\pi^2\rho^2\sin^2(\theta-\phi)} d\theta.$$

C. No A Priori

We consider the case of a source DOA uniformly distributed over $[-\pi, \pi]$. There is actually an infinity of equivalent solutions. In fact, because $1/F(\theta)$ is being integrated over one period, it can be shown that C is unchanged by a translation of ϕ. Hence, we assume $\phi = 0$ within this section. A sample cost function C (for $\beta = 0.8$) is presented in Fig. 2, showing that optimality is met at $\psi_1 = -\psi_2 = \pi/2$, which is verified for all possible values of β. In general, optimality is met with the two sensors pointing in opposite directions, orthogonally to the axis linking them. This axis, however, can be randomly oriented. We denote with CAMU the two-sensor array depicted in Fig. 3 and characterized by $\phi = 0$, $\psi_1 = \pi/2$, and $\psi_2 = -\pi/2$. It is optimal for a source with a uniformly distributed DOA.

Contrary to the two-sensor UCA, the CAMU array does not have an infinite CRB at any direction, as is clear from Fig. 4. As a consequence, its accuracy (in terms of the ECRB) is finite, of the same order as that of the three-sensor UCA. Also, Fig. 4(a) shows that, as the β of the constituent sensors increases, the CRB is reduced in the end-fire direction and increased at broadside. A good compromise seems to be attained for β values around 0.5, where the CRB fluctuates the least and the CAMU is closest to being isotropic. This would be the best design for those applications requiring (more or less) the same accuracy at all possible look directions.

As can be concluded from Fig. 5, the use of directional sensors is more beneficial to CAMU than to UCA. With this particular configuration of the CAMU array, substituting $\phi = 0$, $\psi_1 = \pi/2$, and $\psi_2 = -\pi/2$ into (17) results in

$$\frac{F(\theta)}{2g_0^2} = \frac{\beta^2\cos^2(\theta)}{1+\beta^2\sin^2(\theta)} + \pi^2\rho^2\sin^2(\theta)\frac{\left[1-\beta^2\sin^2(\theta)\right]^2}{1+\beta^2\sin^2(\theta)}, \tag{18}$$

which is not zero in any direction as long as β is not 0. Again, from Fig. 5, the best performance is obtained using sensors with β values slightly larger than 0.5. As can be concluded from Fig. 5, the optimally configured two-sensor array is outperformed by the larger three-sensor UCA. However, this is true only because, disadvantageously, this pdf expresses no a priori about the source DOA. As shown in the next section, the situation is more profitable to our design if (more) information is available about the source DOA.

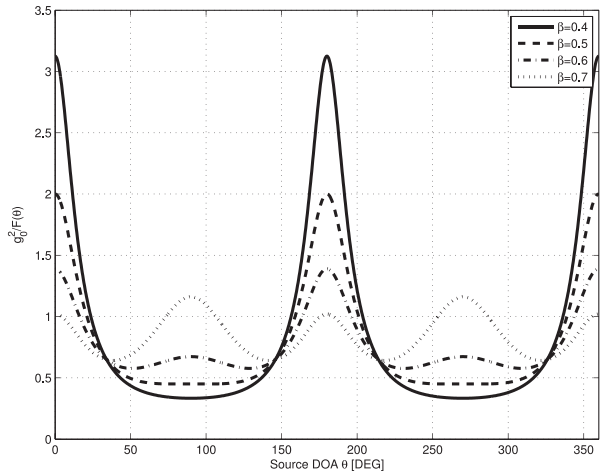

(a)

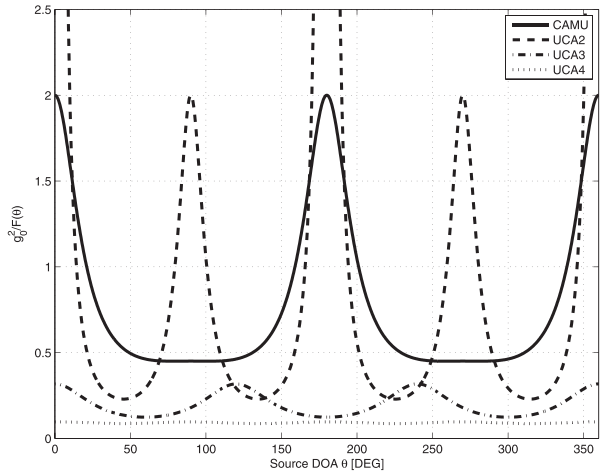

(b)

Fig. 4. Values of $g_0^2/F(\theta)$ (which is proportional to CRB), for all possible source DOAs, for both CAMU array in (a) and (b) and reference UCAs in (b). In (b), $\beta = 0.5$.

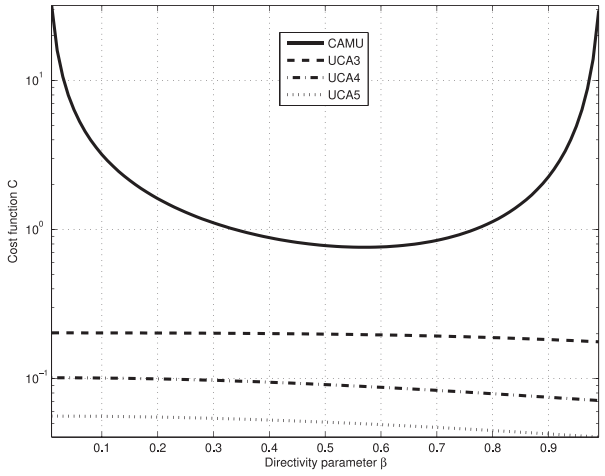

Fig. 5. Compared performance of CAMU and UCA in terms of cost function C (proportional to ECRB) as function of β (expressing directivity of cardioid sensor), for uniformly distributed source DOA.

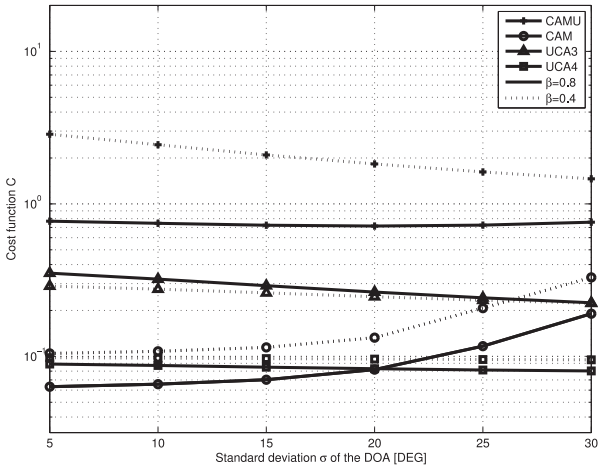

(a) Performance of the optimized CAM array

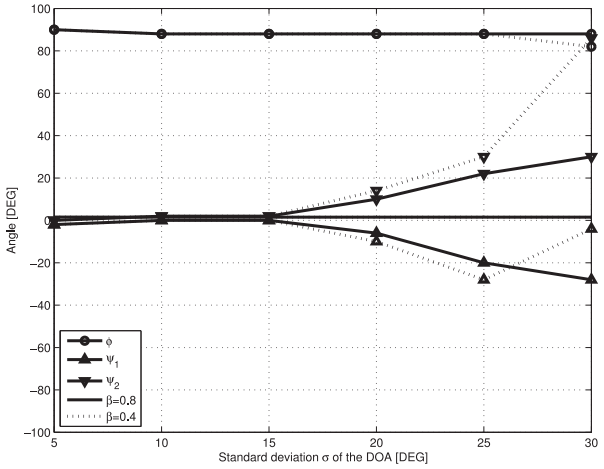

(b) Shape of the optimized CAM array

Fig. 6. Performance (a) and shape (b) of optimized CAM array, compared to nonadaptive fixed-geometry CAMU and UCA arrays, for zero-mean normally distributed source DOA with standard deviation as shown along horizontal axis.

D. Normal A Priori

In some realistic scenarios, the source DOA is expected to appear in a given direction Ω that is assumed, without loss of generality, to be 0. The DOA is modeled as a centered normal random variable, and the optimal two-sensor array is studied as function of the standard deviation σ. The geometry and performance of the optimal CAM array are shown in Fig. 6 for $\sigma \leq 40$ deg, in order to ensure that the pdf $f(\theta) = (1/\sqrt{2\pi}\sigma)\exp[-\theta^2/(2\sigma^2)]$ is almost zero for any θ not in $[-\pi, \pi]$. Results shown in Fig. 6(a) suggest that there is a range of σ where the optimized two-sensor array achieves a performance close to (better and worse than) that of the three-sensor UCA. In this case, the two sensors of the optimized array are placed orthogonally ($\phi = \pi/2$) to the expected source DOA and are pointing into symmetric (with respect to the DOA) directions ($\psi_1 = -\psi_2$). The larger the uncertainty σ about

Ω, the larger the offset $|\psi_1| = |\psi_2|$, as shown in Fig. 6(b). However, for an excessively large σ (i.e., limited a priori information), geometry optimization is less beneficial and performance is not much better than that of the CAMU array.

E. Arbitrary A Priori

A more general pdf model is that of a mixture of Gaussian distributions with different means (that express the different look directions) and variances (that express the uncertainty about the look directions). Strictly speaking, we let P be the number of look directions. We let κ_p, Ω_p, and σ_p be the weight, mean, and standard deviation relative to the pth distribution, so that for any θ in $[-\pi, \pi]$, $\sum_{p=1}^{P} \kappa_p = 1$. We assume $-\pi < \Omega_p - 3\sigma_p$ and $\Omega_p + 3\sigma_p < \pi$ for all p in order to have $\sum_{p=1}^{P} (\kappa_p/\sigma_p\sqrt{2\pi}) \exp[-(\theta - \Omega_p)^2/(2\sigma_p^2)] \simeq 0$ for any θ not in $[-\pi, \pi]$. In the simulations, we have assumed equally likely look directions—i.e., $\kappa_1 = \cdots = \kappa_P = 1/P$—and the same uncertainty $\sigma_1 = \cdots = \sigma_P = 10$ deg:

$$f(\theta) = \sum_{p=1}^{P} \frac{\kappa_p}{\sigma_p\sqrt{2\pi}} \exp\left[-\frac{(\theta - \Omega_p)^2}{2\sigma_p^2}\right].$$

In a first set of simulations, and in order to explore the potential of the proposed optimized array for arbitrary pdfs, we assume two possible look directions Ω_1 and Ω_2. Without loss of generality (and in order to obtain an even pdf), we choose $\Omega_1 = -\Omega_2$, ranging from 10 to 90 deg. As illustrated in Fig. 7, we compare the performance of the optimized two-sensor array (CAM) to those of the non-optimized arrays (the two-sensor CAMU and UCAs of three, four, and five sensors). We realize that, overall, the optimized two-sensor array performs similarly to the three-sensor UCA. The CAMU array, which has a minimum size and a nonadaptive geometry, is distinctively the one with the lowest performance.

To illustrate a more irregular pdf, we consider the example where $\Omega_1 = 20$, $\Omega_2 = 50$, and $\Omega_3 = 80$ deg. If sensors with $\beta = 0.8$ are to be used, then it is found that the source thus distributed is best localized using the optimized two-sensor array characterized by $\phi = -40$, $\psi_1 = 48$, and $\psi_2 = 50$ deg. Such an array achieves a performance, in terms of C, equal to 0.092. Naturally, it performs much better than the CAMU array, for which C equals 1.2245. Interestingly, performance is in between those of the three-sensor UCA ($C = 0.1536$) and the four-sensor UCA ($C = 0.0792$).

V. CONCLUSION

We form an array of two directional sensors and use it to estimate the DOA of a distant coplanar source. Sensors are positioned and oriented in order to benefit from the a priori information about the DOA angle and, subsequently, reduce the estimation error. If no a priori is available, a default (CAMU) geometry has the advantage of having a finite precision in every direction. If some (normal) a priori is available, the optimal array geometry (calculated off-line) delivers an accuracy comparable to that of a three- or four-sensor UCA.

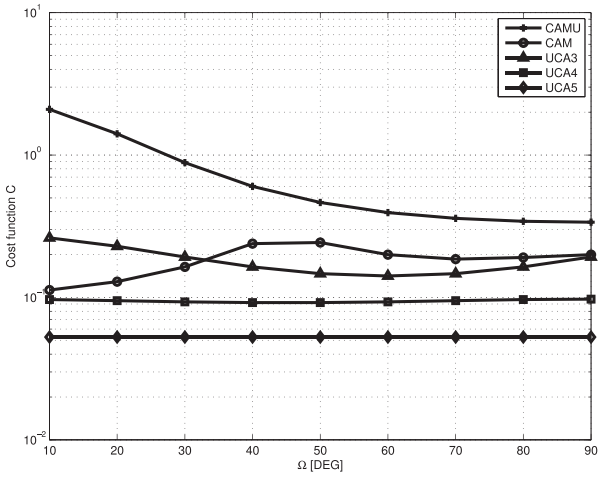

(a)

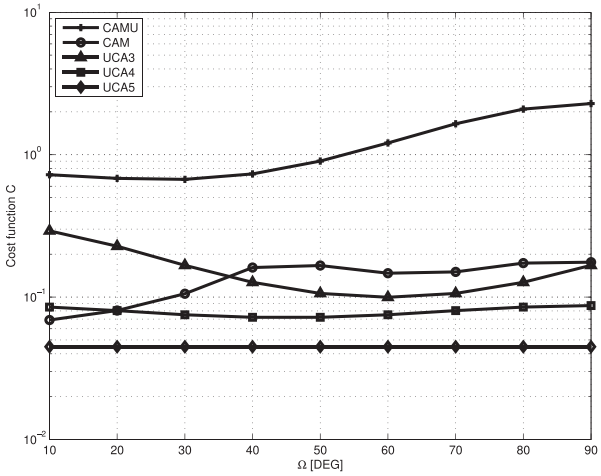

(b)

Fig. 7. Performance of optimal array, compared to nonadaptive CAMU and UCA arrays, for source pdf characterized by two look directions $\pm\Omega$, with $\Omega = 10, 20, \ldots, 90$ deg. Sensors are such that $\beta = 0.4$ in (a) and 0.8 in (b).

APPENDIX A. PROOF OF (5)

Derivation of the ARV, as expressed in (4), leads to $\mathbf{a}'(\theta) = [g_1'(\theta), g_2'(\theta)\exp[2j\pi\rho\cos(\theta - \phi)] - g_2(\theta)2j\pi\rho\sin(\theta - \phi)\exp[2j\pi\rho\cos(\theta - \phi)]]^{\mathrm{T}}$, so that we obtain $\|\mathbf{a}(\theta)\|^2 = g_1^2(\theta) + g_2^2(\theta)$ and $\|\mathbf{a}'(\theta)\|^2 = [g_1'(\theta)]^2 + [g_2'(\theta)]^2 + g_2^2(\theta)4\pi^2\rho^2\sin^2(\theta - \phi)$. Also, $\mathbf{a}'^{\mathrm{H}}(\theta)\mathbf{a}(\theta) = g_1(\theta)g_1'(\theta) + g_2(\theta)g_2'(\theta) + 2j\pi\rho g_2^2(\theta)\sin(\theta - \phi)$ results in $|\mathbf{a}'^{\mathrm{H}}(\theta)\mathbf{a}(\theta)|^2 = g_1^2(\theta)[g_1'(\theta)]^2 + g_2^2(\theta)[g_2'(\theta)]^2 + 2g_1(\theta)g_1'(\theta)g_2(\theta)g_2'(\theta) + 4\pi^2\rho^2 g_2^4(\theta)\sin^2(\theta - \phi)$. After substitution into (3), we update

$\|\mathbf{a}(\theta)\|^2 F(\theta)$ as follows:

$$\begin{aligned}
&\left[g_1^2(\theta)+g_2^2(\theta)\right]F(\theta)\\
&\quad=g_1^2(\theta)\left[g_1'(\theta)\right]^2+g_1^2(\theta)\left[g_2'(\theta)\right]^2\\
&\qquad+g_1^2(\theta)\,g_2^2(\theta)\,4\pi^2\rho^2\sin^2(\theta-\phi)+g_2^2(\theta)\left[g_1'(\theta)\right]^2\\
&\qquad+g_2^2(\theta)\left[g_2'(\theta)\right]^2+g_2^4(\theta)\,4\pi^2\rho^2\sin^2(\theta-\phi)\\
&\qquad-g_1^2(\theta)\left[g_1'(\theta)\right]^2-g_2^2(\theta)\left[g_2'(\theta)\right]^2\\
&\qquad-2g_1(\theta)\,g_1'(\theta)g_2(\theta)\,g_2'(\theta)-4\pi^2\rho^2g_2^4(\theta)\sin^2(\theta-\phi)\\
&\quad=\left[g_1(\theta)\,g_2'(\theta)-g_2(\theta)\,g_1'(\theta)\right]^2\\
&\qquad+4\pi^2\rho^2g_1^2(\theta)\,g_2^2(\theta)\sin^2(\theta-\phi),
\end{aligned}$$

which is equivalent to

$$\begin{aligned}
&\frac{g_1^2(\theta)+g_2^2(\theta)}{g_1^4(\theta)}F(\theta)\\
&\quad=\left\{\left[\frac{g_2(\theta)}{g_1(\theta)}\right]'\right\}^2+4\pi^2\rho^2\frac{g_2^2(\theta)}{g_1^2(\theta)}\sin^2(\theta-\phi)
\end{aligned}$$

and so to (5).

APPENDIX B. PROOF OF (10)

For the considered UCA, the ARV (1) given by $[\mathbf{a}(\theta)]m=g(\theta-\phi_m)\exp[j2\pi R\lambda\cos(\theta-\phi_m)]\stackrel{\wedge}{=}g_m\exp(j\tau_m)$ results in (3) being transformed into

$$\begin{aligned}
F(\theta)=&\sum_{m=1}^{M}g_m'^2+\sum_{m=1}^{M}g_m^2\tau_m'^2\\
&-\frac{\left(\sum_{m=1}^{M}g_mg_m'\right)^2+\left(\sum_{m=1}^{M}g_m^2\tau_m'\right)^2}{\sum_{m=1}^{M}g_m^2}.
\end{aligned}$$

Using (8), we prove the following identities: $\sum_{m=1}^{M}\sin[k(\theta-\phi_m)]=0$ for $M>k\geq 1$, $\sum_{m=1}^{M}\sin[k(\theta-\phi_m)]\cos[l(\theta-\phi_m)]=0$ for $M>k+1\geq 2$, and $\sum_{m=1}^{M}\sin(\theta-\phi_m)\cos[k(\theta-\phi_m)]\cos[l(\theta-\phi_m)]=0$ for $M>1+k+l\geq 3$. In turn, this allows us to prove, after simple algebraic manipulations, that for $M>2K+1$,

$$\left(\sum_{m=1}^{M}g_mg_m'\right)^2+\left(\sum_{m=1}^{M}g_m^2\tau_m'\right)^2=0.$$

Now, using

$$\begin{aligned}
&\sum_{m=1}^{M}\sin[k(\theta-\phi_m)]\sin[l(\theta-\phi_m)]\\
&\quad=\sum_{m=1}^{M}\cos[k(\theta-\phi_m)]\cos[l(\theta-\phi_m)]\\
&\quad=\begin{cases}M/2 & \text{for } M>k+l\geq 2,\ k=l\\ 0 & \text{for } M>k+l\geq 2,\ k\neq l\end{cases}
\end{aligned}$$

$$\begin{aligned}
&\sum_{m=1}^{M}\cos[2(\theta-\phi_m)]\cos[k(\theta-\phi_m)]\\
&\quad=\begin{cases}M/2 & \text{for } M>k+2\geq 3,\ k=2\\ 0 & \text{for } M>k+2\geq 3,\ k\neq 2\end{cases}
\end{aligned}$$

$$\begin{aligned}
&\sum_{m=1}^{M}\cos[2(\theta-\phi_m)]\cos[k(\theta-\phi_m)]\cos[l(\theta-\phi_m)]\\
&\quad=\begin{cases}M/4 & \text{for } M>k+l+2\geq 4,\ k=l=1\\ M/4 & \text{for } M>k+l+2\geq 4,\ |k-l|=2\\ 0 & \text{for } M>k+l+2\geq 4,\ |k-l|\neq 2,\\ & l\neq 1,k\neq 1\end{cases},
\end{aligned}$$

we can reach the final result in (10).

APPENDIX C. PROOF OF (11)

First, $\max_\theta g_0^2(1+\cos(\theta))^{2K}=2^{2K}g_0^2$. By applying the binomial equality twice to $(1+\cos(\theta))^{2K}=(1/2^{2K})[2+(e^{j\theta}+e^{-j\theta})]^{2K}$, we obtain

$$\begin{aligned}
&(1+\cos(\theta))^{2K}\\
&\quad=\frac{1}{2^{2K}}\left[\sum_{k=0}^{2K}\sum_{\ell=0}^{k}2^{2K-k}\binom{2K}{k}\binom{k}{\ell}e^{j(2l-k)\theta}\right].
\end{aligned}$$

Using the Euler relationship (8),

$$\frac{1}{2\pi}\int_0^{2\pi}(1+\cos(\theta))^{2K}d\theta=\frac{1}{2^{2K}}\sum_{n=0}^{K}2^{2(K-n)}\binom{2K}{2n}\binom{2n}{n}$$

with

$$\binom{a}{b}\stackrel{\wedge}{=}\frac{a!}{b!\,(a-b)!}$$

concludes the proof.

APPENDIX D. PROOFS OF (13)–(16)

By extensive use of (8), we can prove, after tedious manipulations, that

$$\begin{aligned}
\frac{\|\mathbf{a}(\theta)\|^2}{Mg_0^2}&=1+\beta^2\frac{1+\delta_{M,2}\cos(2\theta)}{2}\\
-\frac{\mathbf{a}^{\mathrm{H}}(\theta)\,\mathbf{a}'(\theta)}{g_0^2}&=0,\quad M>3\\
&=j\frac{3}{2}\pi R\beta^2\sin(3\theta),\quad M=3\\
&=\beta(\beta+4j\pi R)\sin(2\theta),\quad M=2
\end{aligned}$$

$$\begin{aligned}
\frac{\|\mathbf{a}'(\theta)\|^2}{Mg_0^2}&=\frac{\beta^2}{2}+\pi^2R^2\left(2+\frac{\beta^2}{2}\right),\quad M\geq 5\\
&=\frac{\beta^2}{2}+\pi^2R^2\left[2+\beta^2\sin^2(2\theta)\right],\quad M=4\\
&=\frac{\beta^2}{2}+\pi^2R^2\left[2+\frac{\beta^2}{2}-2\beta\cos(3\theta)\right],\ M=3\\
&=\beta^2\sin^2(\theta)+\pi^2R^2\left(4+\beta^2\right)\sin^2(2\theta),\ M=2,
\end{aligned}$$

where $\delta_{ij} = 1$ if $i = j$, and 0 otherwise. This can be used to calculate the exact CRB of the UCA, as expressed by (2) and (3), leading to expressions (13)–(16).

HOUCEM GAZZAH
Dept. of Electrical and Computer Engineering
University of Sharjah
M9-223, University City, Sharjah, 27272
United Arab Emirates
E-mail: (hgazzah@sharjah.ac.ae)

JEAN PIERRE DELMAS
Telecom SudParis
CNRS UMR 5157, Université Paris Saclay
9 Rue Charles Fourier
Evry, 91011
France
E-mail: (jean-pierre.delmas@it-sudparis.eu)

SÉRGIO M. JESUS
LARSyS
Universidade do Algarve
Faro, 8005-139
Portugal
E-mail: (sjesus@ualg.pt)

REFERENCES

[1] Krim, H., and Viberg, M.
Two decades of array signal processing research: The parametric approach.
IEEE Signal Processing Magazine, **13**, 4 (July 1996), 67–94.

[2] Lange, O., and Yang, B.
Optimization of array geometry for direction-of-arrival estimation using a priori information.
Advances in Radio Science, **8** (2010), 87–94.

[3] Gazzah, H.
Optimum antenna arrays for isotropic direction finding.
IEEE Transactions on Aerospace and Electronic Systems, **47**, 2 (Apr. 2011), 1482–1489.

[4] Gazzah, H., and Delmas, J. P.
Direction finding antenna arrays for the randomly located source.
IEEE Transactions on Signal Processing, **60**, 11 (Nov. 2012), 6063–6068.

[5] Gazzah, H., and Delmas, J. P.
CRB-based design of linear antenna arrays for near-field source localization.
IEEE Transactions on Antennas and Propagation, **62**, 4 (Apr. 2014), 1965–1974.

[6] Schmidt, R.
Multiple emitter location and signal parameter estimation.
IEEE Transactions on Antennas and Propagation, **34**, 3 (Mar. 1986), 276–280.

[7] Gazzah, H., and Delmas, J. P.
Spectral efficiency of beamforming-based parameter estimation in the single source case.
In *2011 IEEE Statistical Signal Processing Workshop*, Nice, France, June 2011, 153–156.

[8] Oktel, Ü., and Moses, R. L.
A Bayesian approach to array geometry design.
IEEE Transactions on Signal Processing, **53**, 5 (May 2005), 1919–1923.

[9] Bevelacqua, P. J., and Balanis, C. A.
Optimizing antenna array geometry for interference suppression.
IEEE Transactions on Antennas and Propagation, **55**, 3 (Mar. 2007), 637–641.

[10] Schmidt, H., Bellingham, J. G., and Bales, J. W.
Mobile underwater arrays, U.S. Patent 5894450, Apr. 13, 1999.

[11] Wang, D., Lermusiaux, P. F. J., Haley, P. J., Eickstedt, D., Leslie, W. G., and Schmidt, H.
Acoustically focused adaptive sampling and on-board routing for marine rapid environmental assessment.
Journal of Marine Systems, **78**, Suppl. (2009), S393–S407.

[12] Jackson, B. R., Rajan, S., Liao, B. J., and Wang, S.
Direction of arrival estimation using directive antennas in uniform circular arrays.
IEEE Transactions on Antennas and Propagation, **63**, 2 (Feb. 2015), 736–747.

[13] Demmel, F.
Practical aspects of design and application of direction-finding systems.
In *Classical and Modern Direction-of-Arrival Estimation*, E. Tuncer and B. Friedlander, Eds. Burlington, MA: Academic Press, 2009, pp. 53–92.

[14] Liao, B., Tsui, K.-M., and Chan, S.-C.
Frequency invariant uniform concentric circular arrays with directional elements.
IEEE Transactions on Aerospace and Electronic Systems, **49**, 2 (Apr. 2013), 871–884.

[15] Balanis, C. A., and Ioannides, P. I.
Introduction to Smart Antennas. San Rafael, CA: Morgan & Claypool, 2007.

[16] Porat, B., and Friedlander, B.
Analysis of the asymptotic relative efficiency of the MUSIC algorithm.
IEEE Transactions on Acoustics, Speech, and Signal Processing, **36**, 4 (Apr. 1988), 532–544.

[17] Kamkar-Parsi, A. H., and Bouchard, M.
Improved noise power spectrum density estimation for binaural hearing aids operating in a diffuse noise field environment.
IEEE Transactions on Audio, Speech, and Language Processing, **17**, 4 (May 2009), 521–533.

[18] Godara, L. C., and Cantoni, A.
Uniqueness and linear independence of steering vectors in array space.
The Journal of the Acoustical Society of America, **70** (1981), 467–475.

[19] Gavish, M., and Weiss, A. J.
Array geometry for ambiguity resolution in direction finding.
IEEE Transactions on Antennas and Propagation, **44**, 6 (June 1996), 889–895.

[20] Biguesh, M., and Gazor, S.
On proper antenna pattern for a simple source detection and localization system.
IEEE Transactions on Antennas and Propagation, **57**, 4 (Apr. 2009), 1073–1080.

[21] Gazzah, H., and Abed-Meraim, K.
Optimum ambiguity-free directional and omnidirectional planar antenna arrays for DOA estimation.
IEEE Transactions on Signal Processing, **57**, 10 (Oct. 2009), 3942–3953.

[22] Del Val, L., Izquierdo, A., Jiménez, M. I., Villacorta, J. J., and Raboso, M.
Analysis of directive sensor influence on array beampatterns.
In *Microwave and Millimeter Wave Technologies: Modern UWB Antennas and Equipment*, I. Mini, Ed. Rijeka, Croatia: InTech, 2010, pp. 229–242.

[23] Ellis, D. D.
Effect of cardioid and limaçon directional sensors on towed array reverberation response.
Canadian Acoustics, **34**, 3 (2006), pp. 102–103.